ACS Photonics

ACS Editors' Choice

Letter

pubs.acs.org/journal/apchd5

50 GBit/s Photodetectors Based on Wafer-Scale Graphene for Integrated Silicon Photonic Communication Systems

Daniel Schall,*[,†] Daniel Neumaier,[†] Muhammad Mohsin,[†] Bartos Chmielak,[†] Jens Bolten,[†] Caroline Porschatis,[†] Andreas Prinzen,[†] Christopher Matheisen,[†] Wolfgang Kuebart,[‡] Bernhard Junginger,[‡] Wolfgang Templ,[‡] Anna Lena Giesecke,[†] and Heinrich Kurz[†]

[†]Advanced Microelectronic Center Aachen (AMICA), AMO GmbH, Otto-Blumenthal-Straße 25, 52074 Aachen, Germany

[‡]Alcatel-Lucent Deutschland AG, Bell Laboratories, Lorenzstraße 10, 70435 Stuttgart, Germany

Supporting Information

ABSTRACT: Optical data links are the backbone of today's telecommunication infrastructure. The integration of electronic and optic components on one chip is one of the most attractive routes to further increase the system performance. Here, we present the fabrication of photodetectors based on CVD-grown graphene on silicon photonic waveguides. The devices operate bias-free in the C-band at 1550 nm and show an extrinsic −3 dB bandwidth of 41 GHz. We demonstrate that these detectors work at data rates up to 50 GBit/s with excellent signal integrity.

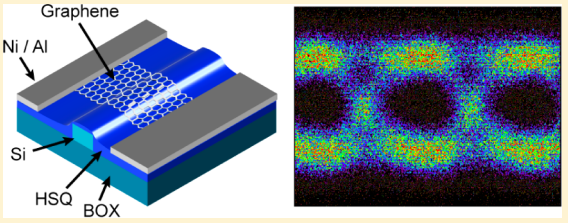

KEYWORDS: *graphene, photodetector, silicon photonic, dark current, data communication, high frequency*

Integrated silicon photonic systems are considered a promising solution for compact data communication systems at infrared wavelengths because of silicon's weak light interaction,[1] the well-developed process technology, and the combination of optical and electrical functionalities on one chip. Photodetectors, key components for these systems, cannot be realized using silicon with satisfying performance, because of silicon's vanishing light absorption at these wavelengths. Currently, the most widely used material to cover this functionality in silicon photonic systems is germanium because it can be grown epitaxially on silicon and absorbs light at the relevant telecommunication O and C bands at 1310 and 1550 nm.[2,3] However, these detectors often show significant dark currents and are intrinsically limited in speed due to the low mobility of charge carriers.[4] The maximum data rate detected by a hybrid integrated germanium photodetector on a silicon waveguide is 40 GBit/s,[5] which has recently been achieved at bias-free operation.[6]

Graphene[7−9] has been considered as an interesting alternative material for photodetectors[10−15] because it shows broadband light absorption ranging from far-infrared to UV,[16] has ultrahigh electron and hole mobilities,[17,18] and can be integrated onto silicon-based systems on wafer-scale.[19] The most widely used concept for graphene photodetectors (GPDs) is based on the photovoltaic charge separation at a graphene−metal interface, where a shift in Fermi's energy is introduced by the metal.[20] These GPDs operate bias-free and are therefore not affected by a dark current and show ultrahigh intrinsic operation speeds of up to 640 GHz,[11,21] good internal quantum efficiencies of 30−60%,[22,23] and a broadband light absorption ranging from wavelengths of 6 μm to 300 nm.[10] While a first high-speed GPD has been successfully integrated on a silicon waveguide operating at a data rate of 12 GBit/s,[24] this device was based on micrometer-sized, microexfoliated graphene, and the data rate was not competitive to state-of-the-art germanium-based photodetectors. In this paper we report on the realization and extensive high-frequency characterization of photovoltaic graphene−metal photodetectors based on wafer-scale graphene grown by chemical vapor deposition integrated on silicon photonic waveguides. These photodetectors show a −3 dB bandwidth of 41 GHz and detect data signals of up to 50 GBit/s.

A schematic of the investigated GPDs is shown in Figure 1a. The photonic base layer consists of 400 nm wide silicon strip waveguides with two grating couplers optimized for the C-band (1550 nm) and TE polarization fabricated on 220 nm thick silicon on an insulator with 3 μm buried oxide. To avoid cracking of the transferred graphene layer at the step edges of the waveguide during device fabrication, a planarization layer of hydrogen silsesquioxane (HSQ) was spin-coated and thermally cured. This HSQ coating process was optimized to achieve a thin layer on top of the waveguide, while preventing suspension of the graphene layer at the waveguide edges. The final thickness of the HSQ layer is 25 nm on top of the waveguide and 130 nm on the rest of the chip. A cross-sectional scanning electron microscopy image of the sample is shown in Figure 1c. The fiber-to-fiber losses of the silicon waveguides and the grating couplers are 13.5 dB on average. Subsequently, a single layer of graphene grown by CVD on a copper substrate was

Received: May 9, 2014
Published: August 14, 2014

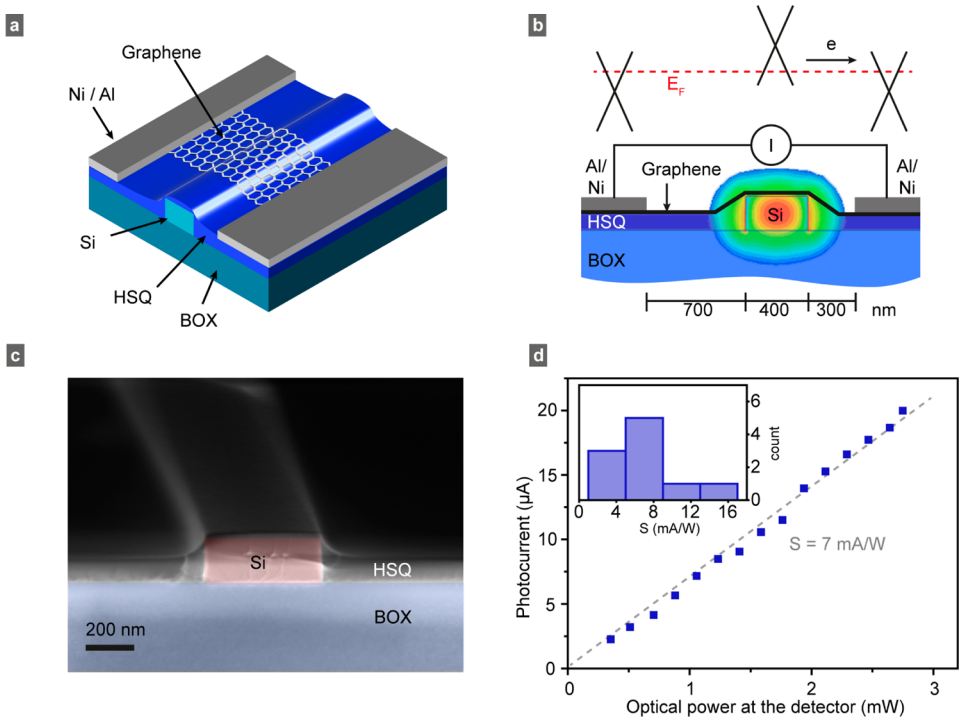

Figure 1. (a) Graphene photodetector integrated on a silicon waveguide with asymmetric contact configuration. (b) Schematic cross section of the device with mode field simulation for the TE mode. The mechanism for charge carrier separation by a pn junction is indicated by the lateral position of the graphene bands. (c) SEM cross section image of a graphene-covered silicon waveguide with an HSQ cladding layer. (d) Photocurrent as a function of the optical power available at the detector with a slope of 7 mA/W. The inset shows the distribution of the sensitivity for 10 devices on this chip.

transferred to the sample by a PMMA transfer method[19] and patterned by oxygen plasma. The length of the graphene layer on the waveguide along the light propagation is 30 μm. The specific evanescent field absorption for this graphene layer on the waveguide, determined in a separate study using the same geometry and different graphene lengths on the waveguide, is 0.06 dB/μm. This results in 35% absorption of the incident light for a 30 μm long GPD. Finally, two contacts per GPD were fabricated by evaporation of 20 nm nickel and 100 nm aluminum and a lift-off technique with separations of 700 and 300 nm from the respective waveguide edges. As derived from measurements on reference transistor structures, the doping level of the graphene introduced by the contacts is n-type, while the doping of the graphene channel in the center of the contacts is p-type. Due to the asymmetric contact scheme, a net photovoltaic photocurrent flow is generated, as the evanescent light is absorbed close to one contact only (only one pn junction), while the second contact is located outside the evanescent field. The mode profile in the fabricated device and the doping levels of the graphene are illustrated in Figure 1b. All measurements were performed at room temperature in normal air, and the GPDs were operated bias-free. Details under bias operation are shown in the Supporting Information.

In order to test the response of the GPDs, infrared light at 1550 nm was coupled into one grating coupler and the photocurrent of the detector was measured using a lock-in amplifier technique. In Figure 1d, the response of one GPD is plotted as a function of the optical power available at the GPD. The power level at the GPD was calculated by subtracting the losses of one grating coupler and the waveguide segment between the grating and the detector (6.75 dB) from the power available at the coupling fiber. The photocurrent shows a linear behavior without saturation and an extrinsic response of 7 mA/W. In total, 10 devices were fabricated and measured on the same chip, showing an extrinsic response ranging from 2 to 16 mA/W, with a mean value of 7 mA/W. A corresponding histogram of the extrinsic response is displayed in the inset of Figure 1d. Taking the finite absorption of the GPD (35%) into account, an absorption normalized extrinsic response ranging from 6 to 46 mA/W can be estimated. The maximum response obtained in this work is comparable to the best value of GPDs based on exfoliated graphene with similar geometry.[24] The variations in the response can be explained by process-induced contaminations on the waveguide, especially from the graphene transfer, leading to a variation of the losses before each photodetector and, hence, different power levels available at the photodetector. Additionally, variations in the contact resistance, the graphene's mobility, and doping level need to be considered. As we do not see a clear correlation between the photoresponse of the GPDs and the experimentally accessible device parameters, i.e., the device resistance, the insertion loss of the device, and the sensitivity of the GPD, we have to assume that the variations in the sensitivity of the GPDs arise by a combination of above-mentioned reasons.

In general, measuring the maximum operation speed of high-speed photodetectors is a delicate task if the frequency response of the actual device is masked by the frequency response of the equipment. In order to explore the full frequency response of our GPDs with minimal parasitic effects, an optical heterodyne technique is used. Two laser sources with narrow bandwidths of 10 MHz are operated at light frequencies f_1 and f_2, respectively, causing an amplitude beating at the difference frequency f_1-f_2. By tuning one laser's frequency, the beating frequency is varied from 1 to 100 GHz, with approximately 1 GHz resolution. The

dx.doi.org/10.1021/ph5001605 | ACS Photonics 2014, 1, 781−784

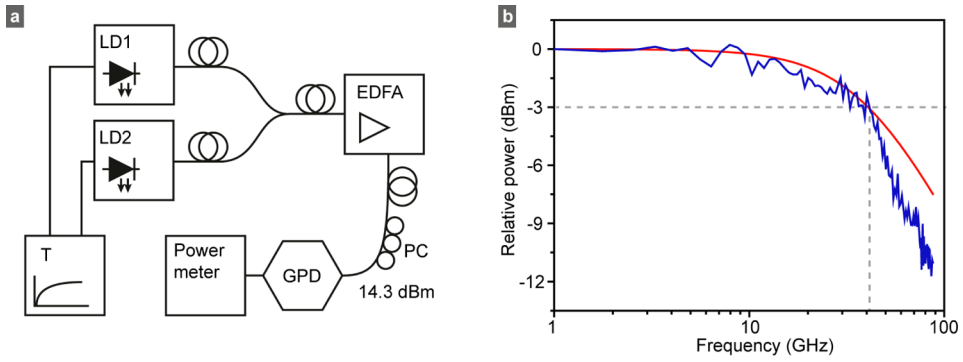

Figure 2. (a) Schematic of the heterodyne measurement setup consisting of laser diodes (LD), an optical amplifier (EDFA), a temperature controller (T), a polarization control unit (PC), a power meter, and the GPD. (b) Frequency response of the relative photodetector output power in dBm with a −3 dB roll-off frequency at 41 GHz (blue). Calculated RC low pass with a −3 dB frequency of 41 GHz (red).

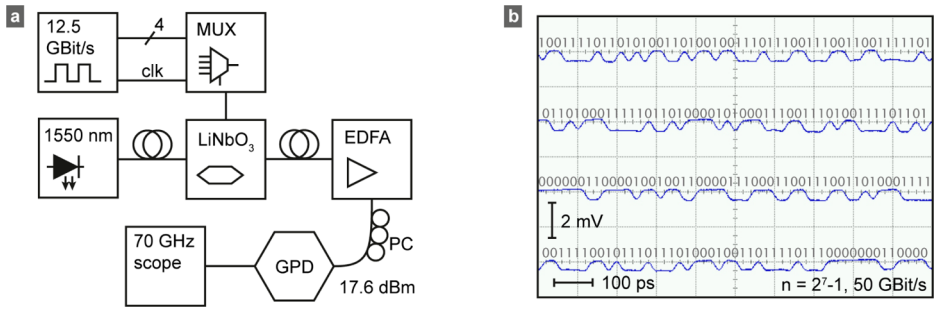

Figure 3. (a) Measurement setup of the 50 GBit/s link, consisting of 4 bit pattern generators including a clock (clk), a multiplexer (MUX), a laser source, a modulator ($LiNbO_3$), an optical amplifier (EDFA), a polarization control unit, a sampling scope, and the GPD. (b) Snapshot of a 50 GBit/s NRZ-OOK bit stream recorded by a 70 GHz scope directly connected to the graphene photodetector. The signal is averaged for noise reduction.

corresponding response of the GPDs is detected by an RF power meter.

A schematic of the setup is shown in Figure 2a, and the spectrum of the two lasers is shown in the Supporting Information. The combined output of the lasers was amplified using an erbium-doped fiber amplifier (EDFA) to an average level of 14.3 dBm and coupled into the waveguide. The GPD RF power detected at 1 GHz was −63 dBm. This value is in accordance with the dc response of the GPD taking the impedance mismatch between the GPD and the power meter into account. In Figure 2b, the relative RF power delivered by the GPD is shown for frequencies up to 87 GHz. The corresponding −3 dB roll-off frequency is 41 GHz, being so far the highest extrinsic value measured for any GPD.[10,11,24,25] The high-frequency equivalent circuit of a GPD consists of the device resistance in parallel to the device and parasitic capacitances forming a resistor−capacitor (RC) component. A corresponding RC low-pass characteristic with a −3 dB frequency of 41 GHz is also plotted in Figure 2b (red line), reproducing well the measured frequency dependence especially below 40 GHz. At higher frequencies, a stronger decrease compared to the calculated RC low-pass characteristic is observed. This deviation can be explained by a drift of the resistance between the probe pads and the probe tip during the measurement (45 min duration) and by a frequency-dependent characteristic of the probe tip used that could not be de-embedded in this setup. In the present design, the total device capacitance is dominated by the pad capacitance, and the graphene channel capacitance can be neglected. On the basis of simulations, the capacitance of the contact pads was calculated. The corresponding −3 dB bandwidth for a device capacitance of 20 fF and the measured resistance of 187 Ω is $f_{-3\ \mathrm{dB}} = 1/2\pi RC = 43$ GHz, which is in excellent agreement with the measured value.

To qualify our GPDs in a data communication system, we integrated the GPDs into an optical 50 GBit/s link sketched in Figure 3a. In this setup a non-return-to-zero on−off keyed (NRZ-OOK) data stream is generated by multiplexing four individual signals at a data rate of 12.5 GBit/s to an optical modulator, generating the 50 GBit/s stream. The optical signal was amplified using an EDFA to an average power of 17.6 dBm and fed into the GPD. The output of the GPD was directly connected to a 70 GHz sampling oscilloscope with 50 Ω input impedance, without any additional amplification to minimize parasitic effects. While this approach enables a close view of the signal generated by the GPD, the signal level at the oscilloscope is low. For this reason, the bit stream directly displayed at the oscilloscope is sample averaged for noise reduction. An open eye diagram recorded in a different setup capable of generating data signals up to 12.5 GBit/s is shown in the Supporting Information. Figure 3b shows four snapshots of an $n = 2^7 - 1$ pseudorandom bit sequence at a data rate of 50 GBit/s. The recorded bit stream in Figure 3b shows excellent signal integrity regarding distortion and signal levels for both "0" and "1" symbols. The 10% to 90% rise time of the signal extracted from the bit stream is approximately 9 ps, corresponding to an effective bandwidth of 39 GHz for the whole setup, which is close to the bandwidth of the photodetector determined above. The short rise time of the whole data link would in principle enable bit rates beyond 50 GBit/s, which, however, could not be generated by the measurement setup.

dx.doi.org/10.1021/ph5001605 | ACS Photonics 2014, 1, 781−784

In summary, we have shown that graphene-based photodetectors with a bandwidth of 41 GHz can be monolithically integrated into silicon photonic systems using wafer-scale CVD-grown graphene. The maximum temperature of 300 °C for our fabrication process is compatible with silicon microelectronic back-end-of-line integration. We demonstrate that data signals up to 50 GBit/s can be detected by the GPDs under zero bias condition, surpassing state-of-the-art germanium-based silicon-waveguide-coupled photodetectors.[5,6] This data rate was limited by the setup, and therefore larger data rates can be expected already for the investigated device. Reducing the parasitic device capacitance will further increase the device speed toward the intrinsic limitations of GPDs. While the maximum extrinsic response of 16 mA/W (46 mA/W absorption normalized) measured in this study is comparable to the response observed in GPDs based on micromechanical exfoliated graphene with similar geometry,[24] the response is behind conventional (nonavalanche type) germanium-based photodetectors (∼1 A/W, corresponding to ∼80% quantum efficiency).[3] However, considering the already measured internal quantum efficiency of GPDs of 30−60%,[22,23] the low response is not an intrinsic limitation of graphene, but can be increased by optimizing the GPD design. Additionally, carrier multiplication in graphene may raise the quantum efficiencies above 100% if specific conditions for carrier multiplication are fullfilled.[26,27] These explicit perspectives for enhancing the performance of GPDs promise an attractive solution for broadband detectors in silicon-based integrated high-speed data communication systems.

■ ASSOCIATED CONTENT

Supporting Information

We show the spectra of the lasers used in the heterodyne setup as well as impulse response measurements of the GPDs, the bias dependency of the photoresponse at 12.5 GBit/s, and an open eye diagram. This material is available free of charge via the Internet at http://pubs.acs.org.

■ AUTHOR INFORMATION

Corresponding Author

*E-mail: schall@amo.de

Notes

The authors declare no competing financial interest.

■ ACKNOWLEDGMENTS

We acknowledge fruitful discussions with Renato Negra and Achim Noculak. This work was financially supported by the German Science Foundation DFG within the SPP 1459 Graphene (project "GraTiS") and by the European Commission under the projects GRAFOL (contract no. 285275) and Flagship Graphene (contract no. 604391).

■ REFERENCES

(1) Jalali, B.; Fathpour, S. Silicon photonics. *J. Lightwave Technol.* **2004**, *24*, 4600−4615.

(2) Bean, J. C. Strained-layer epitaxy of germanium-silicon alloys. *Science* **1985**, *230*, 127−131.

(3) Michel, J.; Liu, J.; Kimerling, L. C. High-performance Ge-on-Si photodetectors. *Nat. Photonics* **2010**, *4*, 527−534.

(4) Bowers, J. E.; Wey, Y. G. High-Speed Photodetectors. In *Handbook of Optics*; Bass, M., Ed.; McGraw-Hill: New York, 1994; p 17.1.

(5) Chen, L.; Lipson, M. Ultra-low capacitance and high speed germanium photodetectors on silicon. *Opt. Express* **2009**, *17*, 7901.

(6) Vivien, L.; Polzer, A.; Marris-Morini, D.; Osmond, J.; Hartmann, J. M.; Crozat, P.; Cassan, E.; Kopp, C.; Zimmermann, H.; Fédéli, J. M. Zero-bias 40 Gbit/s germanium waveguide photodetector on silicon. *Opt. Express* **2012**, *20*, 1096.

(7) Novoselov, K. S.; Geim, A. K.; Morozov, S. V.; Jiang, D.; Zhang, Y.; Dubonos, S. V.; Grigorieva, I. V.; Firsov, A. A. Electric field effect in atomically thin carbon films. *Science* **2004**, *306*, 666.

(8) Novoselov, K. S.; Geim, A. K.; Morozov, S. V.; Jiang, D.; Katsnelson, M. I.; Grigorieva, I. V.; Dubonos, S. V.; Firsov, A. A. Two-dimensional gas of massless Dirac fermions in graphene. *Nature* **2005**, *438*, 197−200.

(9) Zhang, Y. B.; Tan, Y. W.; Stormer, H. L.; Kim, P. Experimental observation of the quantum Hall effect and Berry's phase in graphene. *Nature* **2005**, *438*, 201−204.

(10) Mueller, T.; Xia, F.; Avouris, P. Graphene photodetectors for high-speed optical communications. *Nat. Photonics* **2010**, *4*, 297−301.

(11) Xia, F.; Mueller, T.; Lin, Y.-M.; Valdes-Garcia, A.; Avouris, P. Ultrafast graphene photodetector. *Nat. Nanotechnol.* **2009**, *4*, 839−843.

(12) Bonaccorso, F.; Sun, Z.; Hasan, T.; Ferrari, A. C. Graphene photonics and optoelectronics. *Nat. Photonics* **2010**, *4*, 611−622.

(13) Furchi, M.; Urich, A.; Pospischil, A.; Lilley, G.; Unterrainer, K.; Detz, H.; Klang, P.; Andrews, A. M.; Schrenk, W.; Strasser, G.; Mueller, T. Microcavity-integrated graphene photodetector. *Nano Lett.* **2012**, *12*, 2773−2777.

(14) Bao, Q.; Loh, K. P. Graphene photonics, plasmonics, and broadband optoelectronic devices. *ACS Nano* **2012**, *6*, 3677−3694.

(15) Echtermeyer, T. J.; Britnell, L.; Jasnos, P. K.; Lombardo, A.; Gorbachev, R. V.; Grigorenko, A. N.; Geim, A. K. Strong plasmonic enhancement of photovoltage in graphene. *Nat. Commun.* **2011**, *2*, 458.

(16) Nair, R. R.; Blake, P.; Grigorenko, A. N.; Novoselov, K. S.; Booth, T. J.; Stauber, T.; Peres, N. M. R.; Geim, A. K. Fine structure constant defines visual transparency of graphene. *Science* **2008**, *320*, 1308.

(17) Bolotin, K. I.; Sikes, K. J.; Jiang, Z.; Klima, M.; Fudenberg, G.; Hone, J.; Kim, P.; Stormer, H. L. Ultrahigh electron mobility in suspended graphene. *Solid State Commun.* **2008**, *146*, 51.

(18) Avouris, P. Graphene: electronic and photonic properties and devices. *Nano Lett.* **2010**, *10*, 4285.

(19) Li, X.; Zhu, Y.; Cai, W.; Borysiak, M.; Han, B.; Chen, D.; Piner, R. D.; Colombo, L.; Ruoff, R. S. Transfer of large-area graphene films for high-performance transparent conductive electrodes. *Nano Lett.* **2009**, *9*, 4359−4363.

(20) Xia, F.; Mueller, T.; Golizadeh-Mojarad, R.; Freitag, M.; Lin, Y.-M.; Tsang, J.; Perebeinos, V.; Avouris, P. Photocurrent imaging and efficient photon detection in a graphene transistor. *Nano Lett.* **2009**, *9*, 1039−1044.

(21) Ulrich, A.; Unterrainer, K.; Mueller, T. Intrinsic response time of graphene photodetectors. *Nano Lett.* **2011**, *11*, 2804−2808.

(22) Park, J.; Ahn, Y. H.; Ruiz-Vargasv, C. Imaging of photocurrent generation and collection in single-layer graphene. *Nano Lett.* **2009**, *9*, 1742−1746.

(23) Freitag, M.; Low, T.; Avouris, P. Increased responsivity of suspended graphene photodetectors. *Nano Lett.* **2013**, *13*, 1644−1648.

(24) Gan, X.; Shiue, R.-J.; Gao, Y.; Meric, I.; Heinz, T. F.; Shepard, K.; Hone, J.; Assefa, S.; Englund, D. Chip-integrated ultrafast graphene photodetector with high responsivity. *Nat. Photonics* **2013**, *7*, 883−887.

(25) Pospischill, A.; Humer, M.; Furchi, M. M.; Bachmann, D.; Guider, R.; Fromherz, T.; Mueller, T. CMOS-compatible graphene photodetector covering all optical communication bands. *Nat. Photonics* **2013**, *4*, 892−896.

(26) Winzer, T.; Malic, E. Impact of Auger processes on carrier dynamics in graphene. *Phys. Rev. B* **2012**, *85*, 241404(R).

(27) Winzer, T.; Knorr, A.; Malic, E. Carrier multiplication in graphene. *Nano Lett.* **2010**, *10*, 4839−4843.